ELASTIC IMPEDANCE PARAMETERIZATION AND INVERSION IN A VERTICAL, ROTATIONALLY INVARIANT FRACTURED HTI MEDIUM

XINPENG PAN[1], GUANGZHI ZHANG[1,2], HUAIZHEN CHEN[3] and XINGYAO YIN[1,2]

[1]*School of Sciences, China University of Petroleum (Huadong), Qingdao, Shandong, P.R. China. panxinpeng1990@gmail.com*
[2]*Laboratory for Marine Mineral Resources, Qingdao National Laboratory for Marine Science and Technology, Qingdao, Shandong, P.R. China.*
[3]*Department of Geoscience, University of Calgary, Calgary, Alberta, Canada.*

(Received October 7, 2016; revised version accepted March 2, 2018)

ABSTRACT

Pan, X.P., Zhang, G.Z., Chen, H.Z. and Yin, X.Y., 2018. Elastic impedance parameterization and inversion in a vertical, rotationally invariant fractured HTI medium. *Journal of Seismic Exploration*, 27: 227-254.

Seismic wave propagating in a purely isotropic background medium containing a single set of vertically aligned fractures exhibits a long-wavelength effective transversely isotropy (HTI) with a horizontal symmetry axis. The estimation of fracture weaknesses is significant for the characterization of anisotropy in a fracture-induced HTI medium. Our goal is to demonstrate an azimuthal elastic impedance inversion approach for fracture characterization by utilizing the observable wide- azimuth seismic reflection data in a vertical, rotationally invariant fractured reservoir. Under the assumption of weak contrast across the interface and weak anisotropy, we first derive the perturbations in elastic stiffness parameters of a weakly HTI medium. Then we derive a linearized PP-wave reflection coefficient in terms of P- and S-wave moduli, density, and fracture weaknesses for the case of a weak-contrast interface separating two weakly HTI media based on the perturbation matrix and scattering function. Using the least square ellipse fitting (LSEF) method to calculate the azimuth of fracture normal, we build a perfect linear relationship between the reflection coefficient and fracture weaknesses. Finally, we propose a novel parameterization method for fracture weaknesses, and derive the elastic impedance variation with angles of incidence and azimuth (EIVAZ) equation. In order to refine the inversion stability and lateral continuity, we implement the EIVAZ inversion in a Bayesian framework incorporating the Cauchy-sparse regularization and the low-frequency information regularization, and the nonlinear iteratively reweighted least squares (IRLS) strategy is employed to solve the linear inversion problem. A test on a real data set indicates that the estimated results agree well with the well log interpretation, and the proposed method appears to generate reliable results for the characterization of fractured reservoirs.

KEY WORDS: fracture-induced HTI medium, rotationally invariant fractures, weak-contrast and weak-anisotropy assumption, quasi-weakness parameters, EIVAZ inversion.

0963-0651/18/$5.00

INTRODUCTION

A carbonate reservoir containing vertically parallel fractures is considered to be a transversely isotropic (HTI) medium with a horizontal symmetry axis (Rüger, 1997, 1998; Thomsen, 2002; Tsvankin and Grechka, 2011). Fractures in reservoirs are treated as a vital storage space and migration pathway of hydrocarbon (Narr et al., 2006; Liu and Martinez, 2012). Fracture weaknesses, which are defined by the linear slip model (Hsu and Schoenberg, 1993; Schoenberg and Sayers, 1995; Bakulin et al., 2000), are related to fracture properties (e.g. fracture density, fillings, etc.). In this paper, a novel parameterization method of facture weaknesses was presented to characterize the fracture properties.

Much work has been done to derive the linearized PP-wave reflection coefficients are in a weakly anisotropic HTI medium. Based on the weakly elastic anisotropy theory (Thomsen, 1986), Tsvankin (1996) introduced a series of P-wave anisotropic notations to characterize the HTI medium. Following Tsvankin (1996), linearized PP-wave reflection coefficients were derived in terms of weakly anisotropic parameters (Rüger, 1997, 1998; Pšenčík and Gajewski, 1998; Pšenčík and Vavryčuk, 1998; Pšenčík and Martins, 2001). However, the scattering of seismic wave propagating in fractured layers should not be negligible (Burns et al., 2007; Yin et al., 2013). Based on the elastic inverse scattering theory, Shaw and Sen (2004, 2006) proposed a different method to derive the linear PP-wave reflection coefficients in terms of perturbation in stiffness matrix for a weakly anisotropic medium. Using the stiffness matrix of HTI media (Schoenberg and Sayers, 1995), we derive a linearized PP-wave reflection coefficient in terms of fracture weaknesses for a weakly anisotropic HTI medium based on the elastic inverse scattering theory.

The estimation of elastic and anisotropic parameters in HTI media is influenced by signal-to-noise-ratio of azimuthal seismic data (Chen et al., 2017; Pan et al., 2017a; 2017b). Elastic impedance (EI) inversion has been widely studied in literatures due to the advantage of angle-stack data, and it has been extended to the anisotropic media (Connolly, 1999; Whitcombe, 2002; Martins, 2006; Chen et al., 2014). However, the weakly anisotropic EI part in the existing anisotropic EI equations represents an exponential correction of EI attributable to weak anisotropy. The inversion accuracy of the weakly anisotropic parameters based on the existing anisotropic EI equation may be influenced enormously due to the expression difference between the isotropic and anisotropic EI parts, and the anisotropic EI part is an exponential correction of EI attributable to weak anisotropy. Hence, a novel EIVAZ parameterization in terms of fracture weakness was proposed to remove the exponential correction of EI attributable to weak anisotropy, which may help to improve the inversion stability. Finally, we proposed a stable EIVAZ inversion method in Bayesian framework with Cauchy-sparse and low-frequency information regularization, where the elastic and anisotropic parameters are estimated by employing the nonlinear iteratively reweighted least squares (IRLS) strategy (Scales and Smith, 2000; Bissantz et al., 2009; Daubechies et al., 2010). A test on a real data set validated that

the proposed method makes a reliable estimation of the fracture weaknesses from observed seismic data.

THEORY AND METHOD

Effective stiffness tensor in a weakly anisotropic HTI medium

Based on the first-order perturbation theory (Pšenčík and Vavryčuk, 1998), the effective elastic stiffness tensor $\boldsymbol{C}$ of a inhomogeneous medium is expressed as the sum of the stiffness tensor of a homogeneous isotropic background medium and that of a perturbation medium (Pšenčík; Shaw and Sen, 2004; Yin et al., 2013; Zong et al., 2015)

$$\boldsymbol{C} = \boldsymbol{C}_b + \Delta\boldsymbol{C} \ , \tag{1}$$

where $\boldsymbol{C}_b$ and $\Delta\boldsymbol{C}$ represent the stiffness tensors of the homogeneous isotropic background medium and the perturbation medium, respectively.

Similarly, the effective elastic stiffness tensor $\boldsymbol{C}$ in a weakly anisotropic medium can be expressed as (Yin et al., 2013)

$$\boldsymbol{C} = \boldsymbol{C}_b + \Delta\boldsymbol{C}_{iso} + \Delta\boldsymbol{C}_{ani}, \tag{2}$$

where $\Delta\boldsymbol{C}_{iso}$ and $\Delta\boldsymbol{C}_{ani}$ represent the stiffness tensors of perturbations in the isotropic and anisotropic parts, respectively.

Based on the linear slip theory (Schoenberg, 1980, 1983), the effective compliance tensor $\mathbf{S}$ of a fracture-induced HTI medium is expressed as the sum of the background compliance $\mathbf{S}_b$ and the excess fracture compliance $\mathbf{S}_f$ (Bakulin et al., 2000; Grechka et al., 2003):

$$\mathbf{S} = \mathbf{S}_b + \mathbf{S}_f . \tag{3}$$

For a single set of vertically aligned fractures with normals parallel to the x_1-axis, the excess fracture compliance $\mathbf{S}_f$ is given by (Bakulin et al., 2000; Grechka et al., 2003)

$$\mathbf{S}_f = \begin{bmatrix} Z_N & 0 & 0 & 0 & Z_{NV} & Z_{NH} \\ 0 & 0 & 0 & 0 & 0 & 0 \\ 0 & 0 & 0 & 0 & 0 & 0 \\ 0 & 0 & 0 & 0 & 0 & 0 \\ Z_{NV} & 0 & 0 & 0 & Z_V & Z_{VH} \\ Z_{NH} & 0 & 0 & 0 & Z_{VH} & Z_H \end{bmatrix}. \tag{4}$$

The subscripts N, V and H represent the normal direction, the vertical tangential direction and the horizontal tangential direction, respectively. The compliances Z_N, Z_V, Z_H, Z_{NV}, Z_{NH} and Z_{VH} are defined to relate the change in displacement across the fracture plane to the corresponding traction (stress) components (Grechka et al., 2003). The dimensionless fracture weaknesses are given by (Grechka et al., 2003)

$$0 \le \delta_N \equiv \frac{M_b Z_N}{1 + M_b Z_N} < 1, \tag{5}$$

$$0 \le \delta_V \equiv \frac{\mu_b Z_V}{1 + \mu_b Z_V} < 1, \tag{6}$$

$$0 \le \delta_H \equiv \frac{\mu_b Z_H}{1 + \mu_b Z_H} < 1, \tag{7}$$

$$0 \le \delta_{NV} \equiv \frac{\sqrt{\mu_b M_b}\, Z_{NV}}{1 + \sqrt{\mu_b M_b}\, Z_{NV}} < 1, \tag{8}$$

$$0 \le \delta_{NH} \equiv \frac{\sqrt{\mu_b M_b}\, Z_{NH}}{1 + \sqrt{\mu_b M_b}\, Z_{NH}} < 1, \tag{9}$$

$$0 \le \delta_{VH} \equiv \frac{\sqrt{\mu_b M_b}\, Z_{VH}}{1 + \sqrt{\mu_b M_b}\, Z_{VH}} < 1. \tag{10}$$

Here M_b and μ_b represent P- and S-wave moduli of the background medium.

Inverting the compliance matrix yields the stiffness matrix $\mathbf{C}$ (Schoenberg and Sayers, 1995; Bakulin et al., 2000), which is related to the background stiffness $\mathbf{C}_b$ and the excess fracture stiffness $\mathbf{C}_f$

$$\boldsymbol{C} \equiv \mathbf{S}^{-1} = \left(\mathbf{S}_b + \mathbf{S}_f\right)^{-1} \approx \boldsymbol{C}_b - \boldsymbol{C}_f, \tag{11}$$

where

$$\boldsymbol{C}_b = \begin{bmatrix} M_b & M_b - 2\mu_b & M_b - 2\mu_b & 0 & 0 & 0 \\ M_b - 2\mu_b & M_b & M_b - 2\mu_b & 0 & 0 & 0 \\ M_b - 2\mu_b & M_b - 2\mu_b & M_b & 0 & 0 & 0 \\ 0 & 0 & 0 & \mu_b & 0 & 0 \\ 0 & 0 & 0 & 0 & \mu_b & 0 \\ 0 & 0 & 0 & 0 & 0 & \mu_b \end{bmatrix}, \tag{12}$$

and

$$\boldsymbol{C}_f = M_b \begin{bmatrix} \delta_N & (1-2g)\delta_N & (1-2g)\delta_N & 0 & \sqrt{g}\delta_{NV} & \sqrt{g}\delta_{NH} \\ (1-2g)\delta_N & (1-2g)^2\delta_N & (1-2g)^2\delta_N & 0 & (1-2g)\sqrt{g}\delta_{NV} & (1-2g)\sqrt{g}\delta_{NH} \\ (1-2g)\delta_N & (1-2g)^2\delta_N & (1-2g)^2\delta_N & 0 & (1-2g)\sqrt{g}\delta_{NV} & (1-2g)\sqrt{g}\delta_{NH} \\ 0 & 0 & 0 & 0 & 0 & 0 \\ \sqrt{g}\delta_{NV} & (1-2g)\sqrt{g}\delta_{NV} & (1-2g)\sqrt{g}\delta_{NV} & 0 & g\delta_V & g\sqrt{g}\delta_{VH} \\ \sqrt{g}\delta_{NH} & (1-2g)\sqrt{g}\delta_{NH} & (1-2g)\sqrt{g}\delta_{NH} & 0 & g\sqrt{g}\delta_{VH} & g\delta_H \end{bmatrix}, \tag{13}$$

in which, $g \equiv \mu_b / M_b = \beta_b^2 / \alpha_b^2$, α_b and β_b represents P- and S-wave velocity of the background medium, which are given by

$$\alpha_b = \sqrt{M_b / \rho_b}, \qquad \beta_b = \sqrt{\mu_b / \rho_b}, \tag{14}$$

where ρ_b represents the background density. Based on the first-order perturbation theory, the perturbation of weakly HTI media over a homogeneous isotropic background is expressed as

$$\begin{aligned} \Delta\boldsymbol{C} &= \Delta\boldsymbol{C}_{iso} + \Delta\boldsymbol{C}_{HTI} \\ &= \begin{bmatrix} \Delta M & \Delta M - 2\Delta\mu & \Delta M - 2\Delta\mu & 0 & 0 & 0 \\ \Delta M - 2\Delta\mu & \Delta M & \Delta M - 2\Delta\mu & 0 & 0 & 0 \\ \Delta M - 2\Delta\mu & \Delta M - 2\Delta\mu & \Delta M & 0 & 0 & 0 \\ 0 & 0 & 0 & \Delta\mu & 0 & 0 \\ 0 & 0 & 0 & 0 & \Delta\mu & 0 \\ 0 & 0 & 0 & 0 & 0 & \Delta\mu \end{bmatrix} \\ &\quad - M_b \begin{bmatrix} \Delta\delta_N & (1-2g)\Delta\delta_N & (1-2g)\Delta\delta_N & 0 & \sqrt{g}\Delta\delta_{NV} & \sqrt{g}\Delta\delta_{NH} \\ (1-2g)\Delta\delta_N & (1-2g)^2\Delta\delta_N & (1-2g)^2\Delta\delta_N & 0 & (1-2g)\sqrt{g}\Delta\delta_{NV} & (1-2g)\sqrt{g}\Delta\delta_{NH} \\ (1-2g)\Delta\delta_N & (1-2g)^2\Delta\delta_N & (1-2g)^2\Delta\delta_N & 0 & (1-2g)\sqrt{g}\Delta\delta_{NV} & (1-2g)\sqrt{g}\Delta\delta_{NH} \\ 0 & 0 & 0 & 0 & 0 & 0 \\ \sqrt{g}\Delta\delta_{NV} & (1-2g)\sqrt{g}\Delta\delta_{NV} & (1-2g)\sqrt{g}\Delta\delta_{NV} & 0 & g\Delta\delta_V & g\sqrt{g}\Delta\delta_{VH} \\ \sqrt{g}\Delta\delta_{NH} & (1-2g)\sqrt{g}\Delta\delta_{NH} & (1-2g)\sqrt{g}\Delta\delta_{NH} & 0 & g\sqrt{g}\Delta\delta_{VH} & g\Delta\delta_H \end{bmatrix}, \end{aligned} \tag{15}$$

where $\Delta M = M - M_b$, and $\Delta\mu = \mu - \mu_b$. In addition, $\Delta\delta_N = \delta_{N2} - \delta_{N1}$, $\Delta\delta_V = \delta_{V2} - \delta_{V1}$, $\Delta\delta_H = \delta_{H2} - \delta_{H1}$, $\Delta\delta_{NH} = \delta_{NH2} - \delta_{NH1}$, $\Delta\delta_{NV} = \delta_{NV2} - \delta_{NV1}$, and $\Delta\delta_{VH} = \delta_{VH2} - \delta_{VH1}$ are the changes in fracture weaknesses across the interface, respectively. The two parts in eq. (15) represent the change in the isotropic background and the perturbation induced by vertically aligned fractures, respectively.

Linearized PP-wave reflection coefficients

To derive linearized PP-wave reflection coefficients of an interface separating two weakly elastic anisotropic media, the reflecting layer elastic parameters and density ρ are appropriately expressed as (Shaw and Sen, 2004)

$$\boldsymbol{c}_{ij} = \boldsymbol{c}_{ij\_b} + \Delta\boldsymbol{c}_{ij}, \tag{16}$$

and

$$\rho = \rho_b + \Delta\rho, \tag{17}$$

where the subscript *b* represents the background medium and the symbol Δ indicates the small perturbation, namely $\left|\Delta c_{ij}/c_{ij}\right| << 1$ and $\left|\Delta\rho/\rho\right| << 1$.

Under the assumption of the small perturbation, the time-harmonic scattered wave-field **u** of the heterogeneous medium given by (Červený, 2001)

$$\mathbf{u}(\mathbf{x},\omega) = \int_V \left[\omega^2 \Delta\rho(\mathbf{x}) u_i^0(\mathbf{x},\omega) G_{ni}^0(\mathbf{x},\omega) - \Delta c_{ij}(\mathbf{x}) \frac{\partial u_k^0(\mathbf{x},\omega)}{\partial x_l} \frac{\partial G_{ni}^0(\mathbf{x},\omega)}{\partial x_j} \right] d\mathbf{x}, \tag{18}$$

where ω represents the circular frequency, and $u_i^0(\cdot)$ and $G_{ni}^0(\cdot)$ represent the elastic wave-field resulting from the exciting source and the Green's function, respectively.

In the case of PP-wave propagation in a homogeneous isotropic background media, the Green's function is given by (Červený, 2001)

$$G_{ni}^0(\mathbf{x},\omega) = \frac{N_n N_i}{4\pi M_b} \frac{1}{\mathbf{r}} e^{iw\mathbf{r}/\sqrt{M_b/\rho_b}}, \tag{19}$$

where **r** represents the source-receiver distance, and N_n and N_i represent the source and receiver directions, respectively.

Using the Born integral and stationary phase method, the linearized PP-wave reflection coefficients for arbitrary anisotropic media embedded in an isotropic background medium are given by (Shaw and Sen, 2004)

$$R_{\mathrm{PP}} = \frac{1}{4\rho_b \cos^2\theta} S(\mathbf{r}_0), \tag{20}$$

where θ is the angle of incidence, $\mathbf{r}_0$ is the point on the horizontal interface, and $\mathbf{S}(\mathbf{r}_0)$ is the scattering function (Eaton and Stewart, 1994; Burridge et al., 1998), which is given by (Shaw and Sen, 2006)

$$S(\mathbf{r}_0) = \Delta\rho\xi + \Delta C_{mn}\eta_{mn} \ , \tag{21}$$

where

$$\xi = \mathrm{t_i t_i'}\Big|_{\mathbf{r}=\mathbf{r}_0} , \tag{22}$$

and

$$\eta_{mn} = \mathrm{t_i' p_j' t_k p_l}\Big|_{\mathbf{r}=\mathbf{r}_0} , \tag{23}$$

in which, p and t represent the slowness vectors and the polarization vectors, respectively. The prime represents the scattered wave. Relationships among the subscripts *m, n, i, j, k* and *l* in eq. (23) are expressed as (Shaw and Sen, 2006)

$$m = i\delta_{ij} + \left(9 - i - j\right)\left(1 - \delta_{ij}\right), \tag{24}$$

and

$$n = k\delta_{kl} + \left(9 - k - l\right)\left(1 - \delta_{kl}\right), \tag{25}$$

where δ_{ij} and δ_{kl} are the Kronecker delta function.

The linearized PP-wave reflection coefficient $R_{pp}(\theta,\phi;\boldsymbol{\delta})$ in terms of fracture weaknesses $\boldsymbol{\delta} = \left[\delta_N,\ \delta_V,\ \delta_H,\ \delta_{NV},\ \delta_{NH},\ \delta_{VH}\right]^T$ for the case of an interface separating two fracture-induced HTI medium is derived as (see Appendix A)

$$R_{pp}(\theta,\phi;\boldsymbol{\delta}) = R_{pp}^{iso}(\theta) + R_{pp}^{ani}(\theta,\phi;\boldsymbol{\delta}), \tag{26}$$

where

$$R_{pp}^{iso}(\theta) = a(\theta)R_M + b(\theta)R_\mu + c(\theta)R_\rho,$$

$$R_{pp}^{ani}(\theta,\phi;\boldsymbol{\delta}) = \frac{1}{2}d(\theta,\phi)\Delta\delta_N + \frac{1}{2}e(\theta,\phi)\Delta\delta_V + \frac{1}{2}f(\theta,\phi)\Delta\delta_H + \frac{1}{2}g(\theta,\phi)\Delta\delta_{NH},$$

$$a(\theta) = \sec^2\theta/2, \quad b(\theta) = -4g\sin^2\theta, \quad c(\theta) = 1-\sec^2\theta/2,$$

$$d(\theta,\phi) = -\sec^2\theta/2\left[2g\sin^2\theta\sin^2\phi + 2g\cos^2\theta - 1\right]^2,$$

$$e(\theta,\phi) = 2g\sin^2\theta\cos^2\phi, \quad f(\theta,\phi) = -2g\sin^2\theta\tan^2\theta\sin^2\phi\cos^2\phi,$$

$$g(\theta,\phi) = 2\sqrt{g}\tan^2\theta\sin\phi\cos\phi\left[1-2g\left(\sin^2\theta\sin^2\phi + \cos^2\theta\right)\right].$$

The quantity θ is the phase angle, which represents the angle between the normal to the interface and the phase vector normal to the incident wave front, and ϕ is the azimuth of the seismic line with respect to the symmetry axis of the fracture system (i.e., $\phi = \phi_{obs} - \phi_{sym}$, which represents the difference between the observation azimuth ϕ_{obs} and the fracture symmetry axis azimuth ϕ_{sym}, as shown in Fig. 1).

In order to obtain the linear expression of eq. (26), the fracture symmetry axis azimuth ϕ_{sym} can be first extracted based on the amplitude inversion method of small incident angle data easily and accurately (Jenner, 2002; Mahmoudian and Margrave, 2012). In this paper, following Rüger (1997, 1998), we use azimuthal gradients to calculate the fracture symmetry axis azimuth ϕ_{sym} based on the least square ellipse fitting (LSEF) method (see Appendix B).

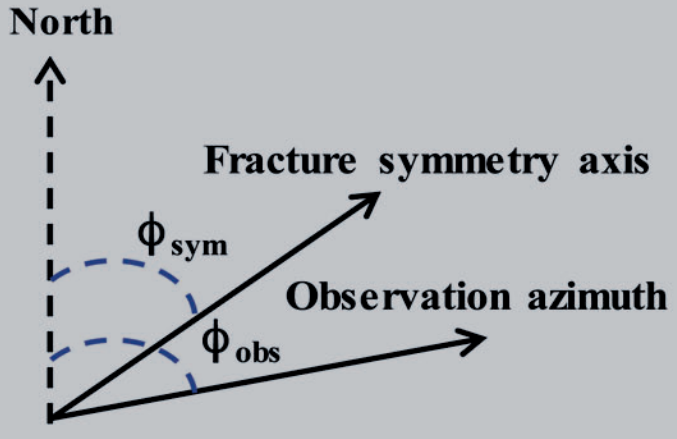

Fig. 1. Azimuth angle with respect to fracture symmetry axis azimuth.

In eq. (26), $R_{pp}^{iso}(\theta)$ and $R_{pp}^{ani}(\theta,\phi)$ represent the background isotropic part and anisotropic part of the reflection coefficient, respectively, and $R_M = \frac{1}{2}\frac{\Delta M}{M_b}$, $R_\mu = \frac{1}{2}\frac{\Delta \mu}{\mu_b}$ and $R_\rho = \frac{1}{2}\frac{\Delta \rho}{\rho_b}$ are the reflectivities of the P- and S-wave moduli and density, respectively. For a set of fractures with properties that are invariant under rotation about the normal to the fracture faces (Schoenberg and Sayers, 1995), the compliances satisfy the relationships given by (Hsu and Schoenberg, 1993)

$$Z_{NV} = Z_{NH} = Z_{VH} = 0, \quad Z_V = Z_H. \tag{28}$$

Substituting eq. (28) into eqs. (5) to (10) yields

$$Z_{NV} = Z_{NH} = Z_{VH} = 0, \quad Z_V = Z_H = Z_T, \tag{29}$$

where δ_T represents the tangential fracture weakness.

Thus eq. (26) is then rewritten as

$$R_{\mathrm{PP}}^{ani}(\theta,\phi;\delta_N,\delta_T) = \frac{1}{2}d(\theta,\phi)\Delta\delta_N + \frac{1}{2}h(\theta,\phi)\Delta\delta_T, \tag{30}$$

where

$$h(\theta,\phi) = 2g\left(\sin^2\theta\cos^2\phi - \sin^2\theta\tan^2\theta\sin^2\phi\cos^2\phi\right). \tag{31}$$

We observe that the background reflectivity term $R_{pp}^{iso}(\theta)$ is related to relative changes in the elastic parameters, which is different from the weakly anisotropic term $\Delta R_{pp}^{ani}(\theta,\phi;\boldsymbol{\delta})$ that is expressed in terms of the changes in fracture weaknesses. The inversion accuracy of elastic and fracture weakness parameters may be influenced enormously due to these two different expressions. Hence, we present a new parameterization method of the normal and tangential fracture weaknesses (see Appendix C)

$$\delta_N^r = \frac{1}{1-\delta_{N0}}\left(\delta_N + 1 - \delta_{N0}\right), \tag{32}$$

and

$$\delta_T^r = \frac{1}{1-\delta_{T0}}\left(\delta_T + 1 - \delta_{T0}\right), \tag{33}$$

where the subscript 0 represents the average quantities. Incorporating the new fracture weaknesses yields

$$R_{\delta_N^r} = \frac{1}{2}\left(\frac{\Delta\delta_N^r}{\delta_{N0}^r}\right) = \frac{1}{2}\Delta\delta_N, \tag{34}$$

and

$$R_{\delta_T^r} = \frac{1}{2}\left(\frac{\Delta\delta_T^r}{\delta_{T0}^r}\right) = \frac{1}{2}\Delta\delta_T, \tag{35}$$

where $R_{\delta_N^r}$ and $R_{\delta_T^r}$ represent the fracture normal and tangential weakness reflectivity, respectively. Therefore, the azimuthal dependent term $\Delta R_{\mathrm{PP}}^{ani}(\theta,\phi)$ is rewritten as

$$R_{\mathrm{PP}}^{ani}(\theta,\phi;\delta_N^r,\delta_T^r) = d(\theta,\phi)R_{\delta_N^r} + h(\theta,\phi)R_{\delta_T^r}. \tag{36}$$

Elastic impedance parameterization for fracture weaknesses

Following Connolly (1999) and Martins (2006), the PP-wave reflection coefficient at horizontal interfaces separating the HTI media can be also defined as

$$R_{\mathrm{PP}}(\theta,\phi) \approx \frac{1}{2}\frac{\Delta EI(\theta,\phi)}{\overline{EI(\theta,\phi)}} \approx \frac{1}{2}\Delta\ln\left(\frac{EI(\theta,\phi)}{EI_0}\right), \tag{37}$$

where EI represents the elastic impedance, and EI_0 represents the medium impedance properties.

The single-interface reflectivity eq. (36) can be extended to a time-continuous reflectivity function (Stolt and Weglein, 1985; Buland and Omre, 2003)

$$\begin{aligned} R_{\mathrm{PP}}(t,\Theta,\phi) &= \frac{1}{2}a(t,\Theta)\frac{\partial}{\partial t}\ln M(t) + \frac{1}{2}b(t,\Theta)\frac{\partial}{\partial t}\ln\mu(t) + \frac{1}{2}c(t,\Theta)\frac{\partial}{\partial t}\ln\rho(t) \\ &\quad + \frac{1}{2}d(t,\Theta,\phi)\frac{\partial}{\partial t}\ln\delta_N^r(t) + \frac{1}{2}h(t,\Theta,\phi)\frac{\partial}{\partial t}\ln\delta_T^r(t) \\ &= \frac{1}{2}\frac{\partial}{\partial t}\ln EI(t,\Theta,\phi). \end{aligned} \tag{38}$$

Taking the integral for eq. (38) then yields

$$\begin{aligned}\ln EI(t,\theta,\phi) = a(t,\theta)\ln M(t) + b(t,\theta)\ln \mu(t) + c(t,\theta)\ln \rho(t) \\ + d(t,\theta,\phi)\ln \delta_N^r(t) + h(t,\theta,\phi)\ln \delta_T^r(t).\end{aligned} \tag{39}$$

The evaluation of eq. (39) gives

$$EI(t,\theta,\phi) = \left[M(t)\right]^{a(t,\theta)} \cdot \left[\mu(t)\right]^{b(t,\theta)} \cdot \left[\rho(t)\right]^{c(t,\theta)} \cdot \left[\delta_N^r(t)\right]^{d(t,\theta,\phi)} \cdot \left[\delta_T^r(t)\right]^{h(t,\theta,\phi)}. \tag{40}$$

Following Whitcombe (2002), we derive the normalized EIVAZ as

$$EI(t,\theta,\phi) = EI^{iso}(t,\theta)\Delta EI_{HTI}^{ani}(t,\theta,\phi), \tag{41}$$

where

$$EI^{iso}(t,\theta) = EI_0 \left[\frac{M(t)}{M_0}\right]^{a(t,\theta)} \cdot \left[\frac{\mu(t)}{\mu_0}\right]^{b(t,\theta)} \cdot \left[\frac{\rho(t)}{\rho_0}\right]^{c(t,\theta)}, \tag{42}$$

and

$$\Delta EI_{HTI}^{ani}(t,\theta,\phi) = \left[\frac{\delta_N^r(t)}{\delta_{N0}^r}\right]^{d(t,\theta,\phi)} \cdot \left[\frac{\delta_T^r(t)}{\delta_{T0}^r}\right]^{h(t,\theta,\phi)}, \tag{43}$$

where EI_0, M_0, μ_0, ρ_0, δ_{N0}^r and δ_{T0}^r represent the average values of the elastic and anisotropic properties, which are estimated by using the well log data or the rock physics experiments.

Martins (2006) and Chen et al. (2014) also derived expressions for anisotropic EI equations

$$EI(t,\theta,\phi) = EI^{iso}(t,\theta)\exp\left[2\int d\Delta R_{pp}(t,\theta,\phi;\mathbf{\delta})\right]. \tag{44}$$

Compared with the *EI* equations derived by Martins (2006) and Chen et al. (2014), eq. (41) eliminates the exponential expression for the weakly anisotropic EI term.

Elastic impedance inversion for fracture weaknesses

The EIVAZ inversion for the elastic parameters (i.e., P- and S-wave moduli, and density) and fracture weaknesses in HTI media includes the estimation of the elastic impedance data sets in different incidence angles and azimuths, and the extraction of the elastic parameters and fracture weaknesses from the estimated elastic impedance data sets. The elastic impedance data sets are estimated by using the constrained sparse spike inversion (CSSI) method (Dolberg et al., 2000; Helgesen et al., 2000).

However, the extraction of the elastic parameters and fracture weakness parameters from the estimated elastic impedance data sets is still a challenge. In order to extract the elastic parameters and fracture weaknesses linearly, the logarithmic expression of eq. (42) is expressed as

$$\ln\left[\frac{EI(t,\theta,\phi)}{EI_0}\right] = a(t,\theta)\ln\left(\frac{M(t)}{M_0}\right) + b(t,\theta)\ln\left(\frac{\mu(t)}{\mu_0}\right) + c(t,\theta)\ln\left(\frac{\rho(t)}{\rho_0}\right) + d(t,\theta,\phi)\ln\left(\frac{\delta_N^r(t)}{\delta_{N0}^r}\right) + h(t,\theta,\phi)\ln\left(\frac{\delta_T^r(t)}{\delta_{T0}^r}\right). \tag{45}$$

Defining $\ln(x/x_0)$ as L_x, we rewrite eq. (43) in terms of matrix forms for the case of M incidence angles and K azimuths

$$\mathbf{L_{EI}} = \mathbf{Gm}, \tag{46}$$

where

$$\mathbf{L_{EI}} = \left[L_{EI}(t,\theta_1,\phi_1) \quad L_{EI}(t,\theta_2,\phi_2) \quad \mathrm{L} \quad L_{EI}(t,\theta_M,\phi_K)\right]^T, \tag{47}$$

$$\mathbf{G} = \begin{bmatrix} a(t,\theta_1) & b(t,\theta_1) & c(t,\theta_1) & d(t,\theta_1,\phi_1) & h(t,\theta_1,\phi_1) \\ a(t,\theta_2) & b(t,\theta_2) & c(t,\theta_2) & d(t,\theta_2,\phi_2) & h(t,\theta_2,\phi_2) \\ \mathrm{M} & \mathrm{M} & \mathrm{M} & \mathrm{M} & \mathrm{M} \\ a(t,\theta_M) & b(t,\theta_M) & c(t,\theta_M) & d(t,\theta_M,\phi_K) & h(t,\theta_M,\phi_K) \end{bmatrix}, \tag{48}$$

and

$$\mathbf{m} = \left[L_M(t) \quad L_\mu(t) \quad L_\rho(t) \quad L_{\delta_N^r}(t) \quad L_{\delta_T^r}(t)\right]^T. \tag{49}$$

There is a strong correlation between the parameters, which may influence the reliability of the inversion results (Downton, 2005). Hence, the parameter decorrelation is employed in the present study. The parameter covariance matrix $\mathbf{Cov_m}$ used for the parameter decorrelation, which is expressed in terms of statistical calculation and rock physics relationships, is

$$\mathbf{Cov_m} = \begin{bmatrix} \sigma^2_{L_M} & \sigma_{L_M L_\mu} & \sigma_{L_M L_\rho} & \sigma_{L_M L_{\Delta_N^r}} & \sigma_{L_M L_{\Delta_T^r}} \\ \sigma_{L_M L_\mu} & \sigma^2_{L_\mu} & \sigma_{L_\mu L_\rho} & \sigma_{L_\mu L_{\Delta_N^r}} & \sigma_{L_\mu L_{\Delta_T^r}} \\ \sigma_{L_M L_\rho} & \sigma_{L_\mu L_\rho} & \sigma^2_{L_\rho} & \sigma_{L_\rho L_{\Delta_N^r}} & \sigma_{L_\rho L_{\Delta_T^r}} \\ \sigma_{L_M L_{\Delta_N^r}} & \sigma_{L_\mu L_{\Delta_N^r}} & \sigma_{L_\rho L_{\Delta_N^r}} & \sigma^2_{L_{\Delta_N^r}} & \sigma_{L_{\Delta_N^r} L_{\Delta_T^r}} \\ \sigma_{L_M L_{\Delta_T^r}} & \sigma_{L_\mu L_{\Delta_T^r}} & \sigma_{L_\rho L_{\Delta_T^r}} & \sigma_{L_{\Delta_N^r} L_{\Delta_T^r}} & \sigma^2_{L_{\Delta_T^r}} \end{bmatrix}, \tag{50}$$

where the diagonal elements of covariance matrix represent the variance of the log-domain elastic and anisotropic reflectivity, and the off-diagonal elements represent the correlation between the unknown parameters. Using the singular value decomposition (SVD) method, the covariance matrix is decomposed as

$$\mathbf{Cov_m} = \mathbf{U}\sum\mathbf{U}^T = \mathbf{U}\begin{bmatrix} \sigma_1^2 & & & & \\ & \sigma_2^2 & & & \\ & & \sigma_3^2 & & \\ & & & \sigma_4^2 & \\ & & & & \sigma_5^2 \end{bmatrix}\mathbf{U}^T, \tag{51}$$

where $\mathbf{U}$ represents the eigenvector, and $\sum$ represents the eigenvalues.

After decorrelation, eq. (46) is expressed as

$$\mathbf{L_{EI}} = \mathbf{G}'\mathbf{m}', \tag{52}$$

where $\mathbf{G}' = \mathbf{G}\cdot\mathbf{U}$ and $\mathbf{m}' = \mathbf{U}^{-1}\mathbf{m}$ represent the coefficient matrix and the inverted parameters after decorrelation, respectively.

In order to generate results with a high resolution for the unknown parameters, we use the Cauchy-sparse regularization (Sacchi and Ulrych, 1995; Downton, 2005; Alemie and Sacchi, 2011) in the construction of the objective function $F(\mathbf{m}')$

$$F(\mathbf{m}') = \left(\mathbf{L_{EI}} - \mathbf{G}'\mathbf{m}'\right)^T\left(\mathbf{L_{EI}} - \mathbf{G}'\mathbf{m}'\right) + \lambda_{Cauchy}\sum_{l=1}^{K}\ln\left(1+\mathbf{m}_l'\right), \tag{53}$$

where K represents the time sampling points, and $\lambda_{Cauchy} = \sigma_n^2/\sigma_m^2$ represents the Cauchy regularization parameter with σ_n^2 indicating the noise variance and σ_m^2 the estimated parameter variance.

The low-frequency components in seismic data are relatively weaker, which are easily affected by the noise. In the objective function, we add the low-frequency information regularization (Zong et al., 2013)

$$F(\mathbf{m}') = \left(\mathbf{L_{EI}} - \mathbf{G}'\mathbf{m}'\right)^T\left(\mathbf{L_{EI}} - \mathbf{G}'\mathbf{m}'\right) + \lambda_{Cauchy}\sum_{l=1}^{K}\ln\left(1+\mathbf{m}_l'\right) + \Psi, \tag{54}$$

where

$$\begin{aligned}\Psi = {} & \lambda_M\left\|\vartheta_M - PL_M\right\|_2^2 + \lambda_\mu\left\|\vartheta_\mu - PL_\mu\right\|_2^2 + \lambda_\rho\left\|\vartheta_\rho - PL_\rho\right\|_2^2 \\ & + \lambda_{\delta_N^r}\left\|\vartheta_{\delta_N^r} - PL_{\delta_N^r}\right\|_2^2 + \lambda_{\delta_T^r}\left\|\vartheta_{\delta_T^r} - PL_{\delta_T^r}\right\|_2^2,\end{aligned} \tag{55}$$

and

$$\vartheta_i = \frac{1}{2}\ln\left(\frac{L_i}{L_{i0}}\right)_i, \quad i = M, \mu, \rho, \delta_N^r, \delta_T^r, \tag{56}$$

where λ represents the regularization parameters of the low-frequency information terms, which may control the stability and lateral continuity of the inversion results, and P represents the integral operator matrix. The objective function becomes nonlinear because of the introduction of the Cauchy-sparse and low-frequency regularization. In the present study, we employ the IRLS strategy (Scales and Smith, 2000; Bissantz et al., 2009; Daubechies et al., 2010) to solve the inversion.

EXAMPLES

Estimation of fracture symmetry axis azimuth based on the LSEF method

In order to obtain the linear expression of eq. (41), we first use the LSEF method to estimate the fracture symmetry axis azimuth ϕ_{sym}. Fig. 2 plots the estimated fracture orientation and fracture density *e*, and Figs. 3 and 4 shows the fracture orientation and density nearby the well, in which the direction of the black solid line indicates the fracture orientation, and the length indicates the fracture development intensity (i.e., fracture density).

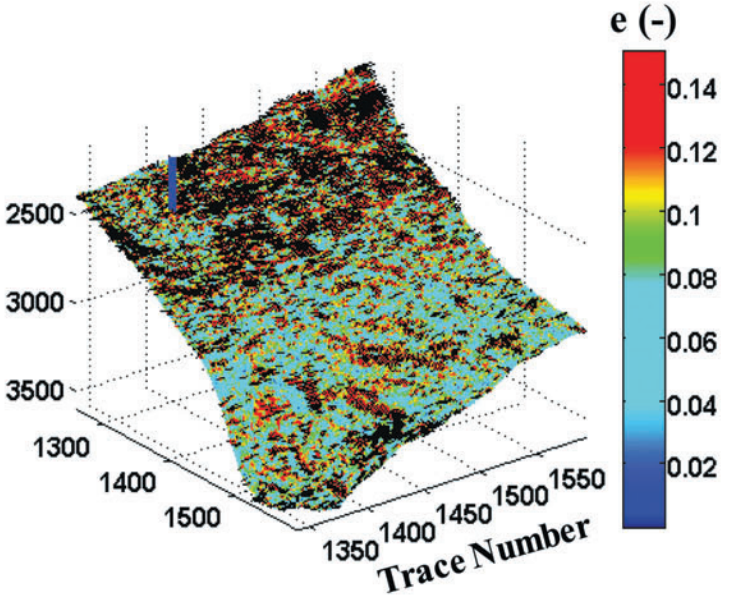

Fig. 2. Estimated fracture orientation and den sity using the LSEF method.

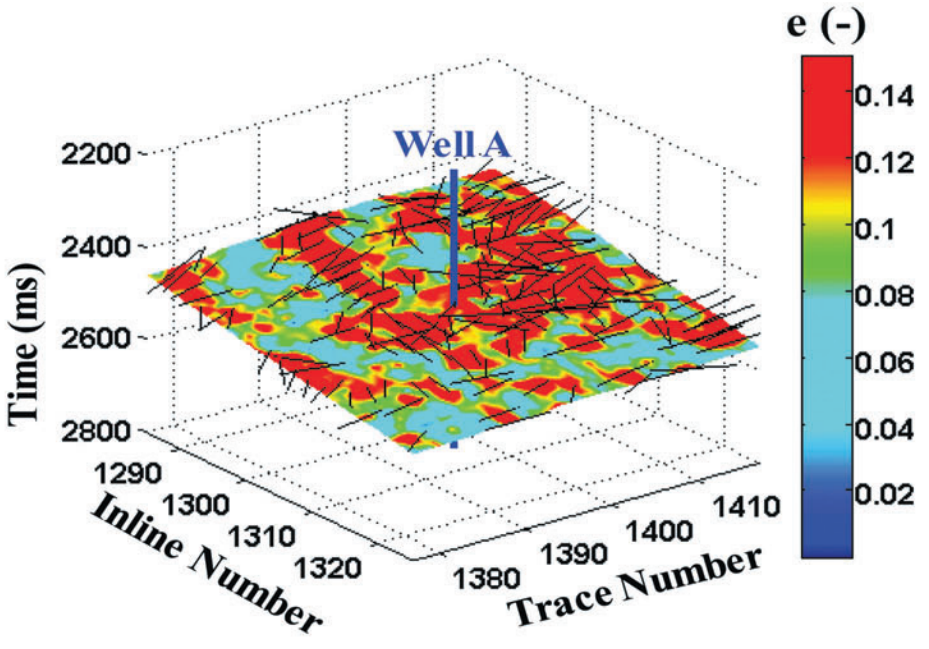

Fig. 3. Estimated fracture orientation and density nearby the well using the LSEF method.

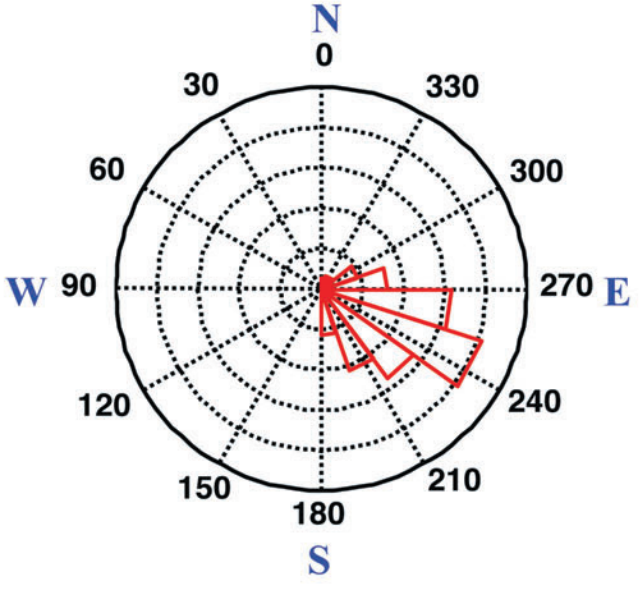

Fig. 4. Estimated fracture symmetry axis azimuth rose diagram nearby the well.

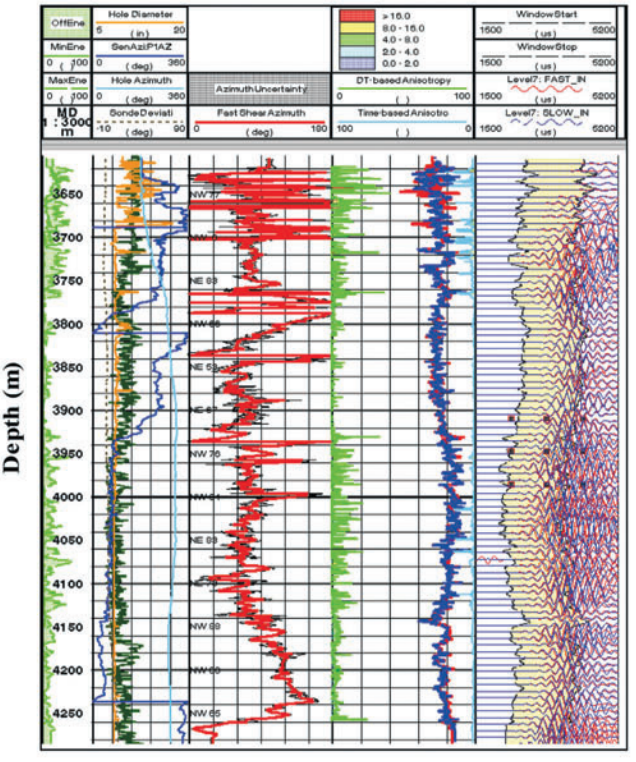

(a)

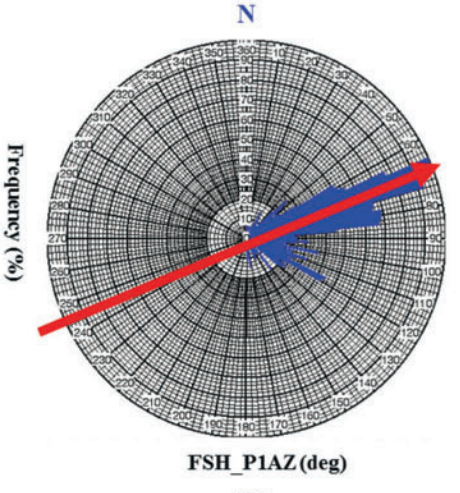

(b)

Fig. 5. Interpreted horizontal maximum stress direction of well A based on the analysis of shear wave anisotropy, where (a) shows the shear wave anisotropic well log; and (b) shows the interpreted horizontal maximum stress direction of well A.

We observe that the fracture symmetry axis azimuth nearby the well A is $\phi_{sym} \approx 240°$, and the direction of fracture development is about SE-NW, which is consistent with the horizontal maximum stress direction of well A shown in Fig. 5. Thus when implementing the azimuthal seismic inversion using the linearized inversion methods, the azimuthal angle ϕ used is equal to the difference between the observation azimuth ϕ_{obs} and the fracture symmetry axis azimuth $\phi_{sym}(240°)$.

Estimation of elastic and anisotropic parameters based on EIVAZ inversion method

A real seismic data set is used to validate the proposed method of EIVAZ inversion for anisotropy in weakly anisotropic HTI media, which is acquired over on an oil-bearing reservoir in East China. The azimuthal angles of this seismic data set are 13° (an average angle of 0°-26°), 45° (an average angle of 23°-66°), 90° (an average angle of 63°-116°), and 135° (an average angle of 113°-156°), as shown in Fig. 6. Before being used in the EIVAZ inversion method, the data are first partially stacked over the incidence angle to generate the near, middle, and far offset/angle data, which may enhance the signal-to-noise ratio of the seismic data. It is important to stress that the seismic data have been processed to preserve the amplitudes, which means the seismic amplitude is considered to be the true response of subsurface reflection interfaces. The target reservoir is a carbonate oil-bearing reservoir around 2.45 seconds at Trace No. 1397. The logging fracture weaknesses are calculated by using well logs and rock physics analysis results (Pan et al., 2017a,b), including the rock minerals and their volume fraction, the porosity of matrix pores, the pore fluid types and water saturation, and the fracture density. Using eq. (41), we can calculate the azimuthal EI information. Fig. 7 shows the estimated EI data at different incidence angles and azimuths, and Figs. 8 and 9 show results of elastic parameters and new-defined fracture weaknesses extracted from the estimated EI data, in which the red solid line indicates the corresponding logging elastic and anisotropic parameters, and the red dashed ellipse indicates the location of the reservoir.

From Fig. 7, we observe that there is a good match between the inversion result of azimuthal EI and the well log curve, which indicates the input for the extraction of elastic parameters and new-defined fracture weaknesses is reliable. From Fig. 8, we observe that the estimated P- and S-wave moduli and density agree with the well log data, and the P- and S-wave moduli are also a sensitive indicator of the target reservoir. Moreover, from Fig. 9, we see that the estimated δ_N^r and δ_T^r related to the normal fracture weakness δ_N and the tangential fracture weakness δ_T show relatively high values, and they may reflect the fracture development zones well. The estimated parameters are consistent with the well log interpretation, which may validate the stability and reliability of the inversion method proposed in this paper. Combining the estimated elastic parameters and the new-defined fracture weaknesses may help to characterize fractured reservoirs.

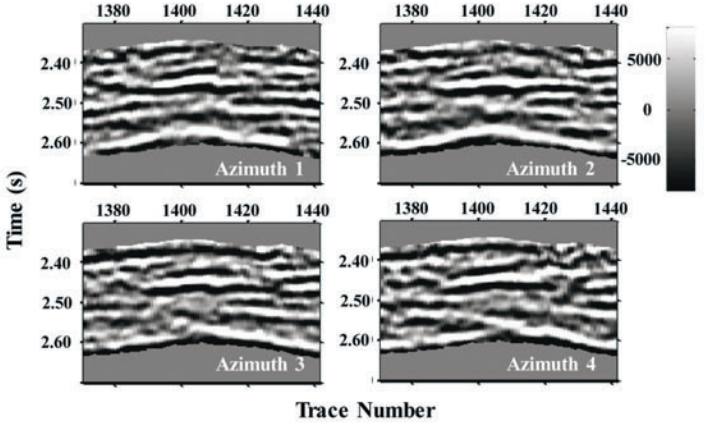

(a)

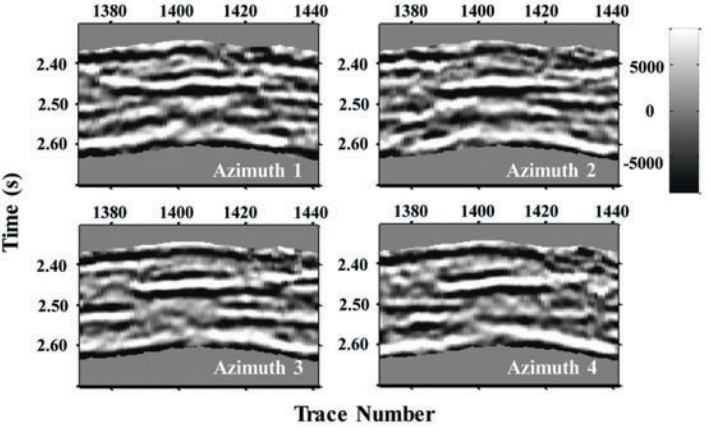

(b)

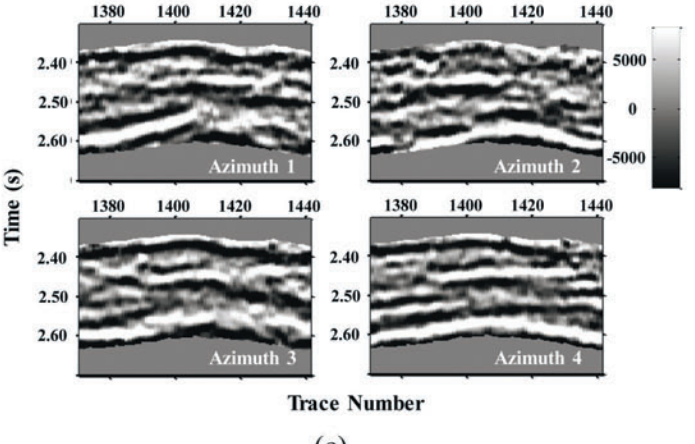

(c)

Fig. 6. Azimuthal seismic data at different angles of incidence, where (a) shows an average angle of 10° (and a range of 5°-15°); (b) shows an average angle of 20° (and a range of 15°-25°); (c) shows an average angle of 30° (and a range of 25°-35°).

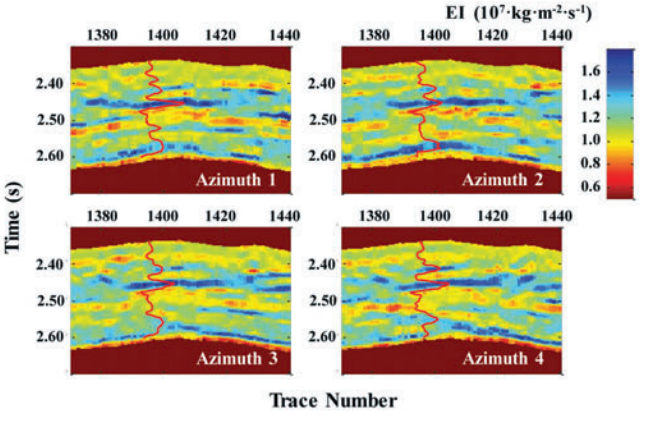

(a)

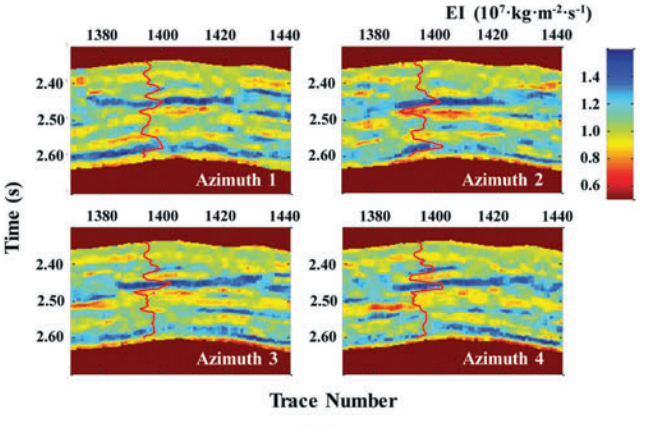

(b)

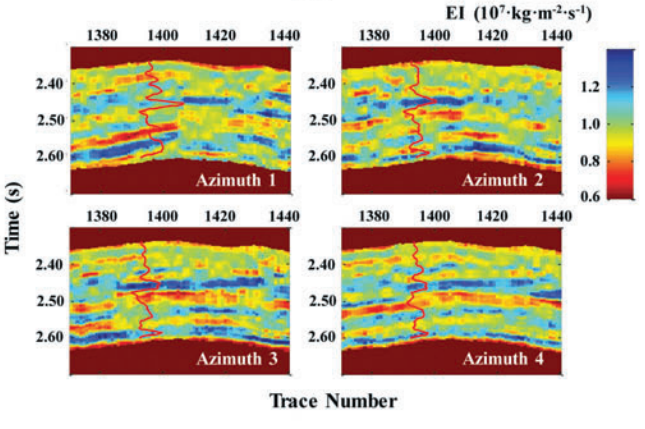

(c)

Fig. 7. Inverted azimuthal EI data at different angles of incidence, where (a) shows an average angle of 10° (and a range of 5°-15°); (b) shows an average angle of 20° (and a range of 15°-25°); (c) shows an average angle of 30° (and a range of 25°-35°).

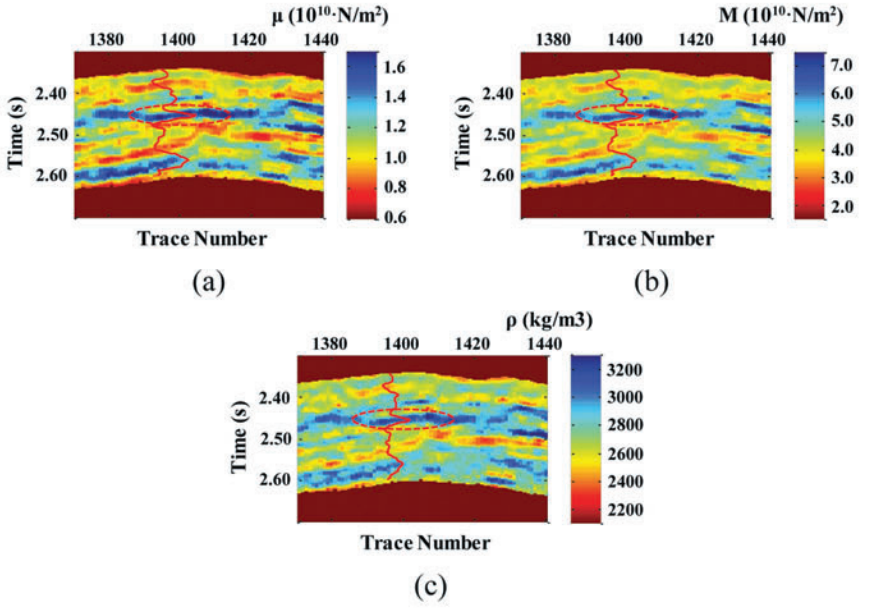

Fig. 8. Extracted elastic parameters based on inverted azimuthal EI data, where (a) shows inverted P-wave moduli M; (b) shows inverted S-wave moduli μ; (c) shows inverted density ρ. Note that the red dashed ellipse indicates the target reservoir.

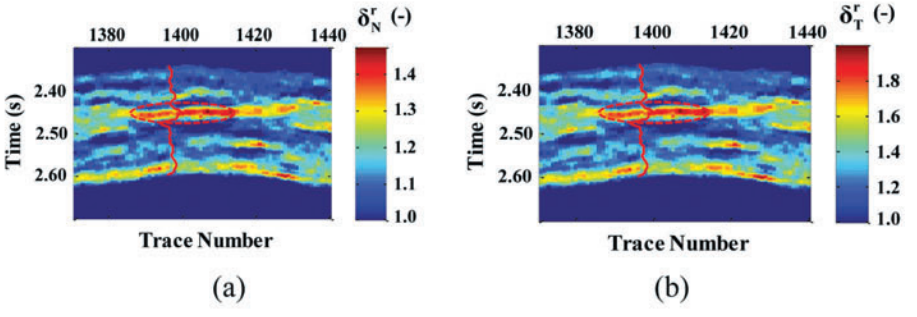

Fig. 9. Extracted fracture weakness parameters based on inverted azimuthal EI data, where (a) shows inverted anisotropic parameter δ_N^r related to the normal fracture weakness δ_N; (b) shows inverted anisotropic parameter δ_T^r related to the tangential fracture weakness δ_T. Note that the red dashed ellipse indicates the target reservoir.

CONCLUSIONS

A single set of vertically parallel fractures forms a common long-wavelength effective HTI anisotropic medium, which are characterized by using the fracture weaknesses. Based on the elastic inverse scattering theory, we first derive a linearized PP- wave reflection coefficient in weakly anisotropic and heterogeneous HTI medium is derived, and then we propose a novel EIVAZ parameterization and inversion method in Bayesian

framework with the Cauchy-sparse and low-frequency regularizations. Finally, the new-defined fracture weaknesses that are related to the normal and tangential fracture weaknesses are estimated by using the nonlinear IRLS strategy. A test on a real data set validate that the proposed method can generate reliable results for the detection of fractured reservoirs. Fluid identification is also important in the characterization of fracture reservoirs. The inversion for fracture fluid factor is a main direction, which is useful to realize the quantitative characterization of fractured oil and gas reservoirs. Applying the EIVAZ method to predict a reasonable fracture fluid factor is a priority for our next study.

ACKNOWLEDGEMENTS

We would like to express our gratitude to the sponsorship of National Natural Science Foundation of China (41674130), National Basic Research Program of China (973 Program, 2014CB239201), National oil and gas major projects of China (2016ZX05027004-001, 2016ZX05002005-009), and the Fundamental Research Funds for the Central Universities (15CX08002A) for their funding in this research. We also thank the anonymous reviewers for their constructive suggestions.

REFERENCES

Alemie, W. and Sacchi, M.D., 2011. High-resolution three-term AVO inversion by means of a Trivariate Cauchy probability distribution. Geophysics, 76: R43-R55.

Bakulin, A., Grechka, V. and Tsvankin, I., 2000. Estimation of fracture parameters from reflection seismic data-Part I: HTI model due to a single fracture set. Geophysics, 65: 1788-1802.

Bissantz, N., Dümbgen, L., Munk, A. and Stratmann, B., 2009. Convergence analysis of generalized iteratively reweighted least squares algorithms on convex function spaces. J. Optimizat., 19: 1828-1845.

Buland, A. and Omre, H., 2003. Bayesian linearized AVO inversion. Geophysics, 68: 185-198.

Burns, D.R., Willis, M.E., Toksöz, M.N., Vetri, L. and Donato, S., 2007. Fracture properties from seismic scattering. The Leading Edge, 26: 1186-1196.

Burridge, R., de Hoop, M.V., Miller, D. and Spencer, C., 1998. Multiparameter inversion in anisotropic media. Geophys. J. Internat., 134: 757-777.

Červený, V., 2001. Seismic Ray Theory. Cambridge University Press, Cambridge.

Chen, H. , Zhang, G., Chen, J. and Yin, X., 2014. Fracture filling fluids identification using azimuthally elastic impedance based on rock physics. J. Appl. Geophys., 110: 98-105.

Chen, H., Zhang, G., Ji, Y. and Yin, X., 2017. Azimuthal seismic amplitude difference inversion for fracture weakness. Pure Appl. Geophys., 174: 279-291.

Connolly, P., 1999. Elastic impedance. The Leading Edge, 18: 438-452.

Daubechies, I., DeVore, R., Fornasier, M. and Güntürk, C.S., 2010. Iteratively reweighted least squares minimization for sparse recovery. Communic. Pure Appl. Mathemat., 63: 1-38.

Dolberg, D.M., Helgesen, J., Hanssen, T.H., Magnus, I., Saigal, G. and Pedersen, B.K., 2000. Porosity prediction from seismic inversion, Lavrans Field, Halten Terrace, Norway. The Leading Edge, 19: 392-399.

Downton, J., 2005. Seismic Parameter Estimation from AVO Inversion. Ph.D. Thesis, University of Calgary.

Eaton, D.W.S. and Stewart, R., 1994. Migration/inversion for transversely isotropic elastic media. Geophys. J. Internat., 119: 667-683.
Grechka, V., Bakulin, A. and Tsvankin, I., 2003. Seismic characterization of vertical fractures described as general linear slip interfaces. Geophys. Prosp., 51: 117-129.
Helgesen, J., Magnus, I., Prosser, S., Saigal, G., Aamodt, G., Dolberg, D. and Busman, S., 2000. Comparison of constrained sparse spike and stochastic inversion for porosity prediction at Kristin Field. The Leading Edge, 19: 400-407.
Hsu, C.J. and Schoenberg, M., 1993. Elastic waves through a simulated fractured medium. Geophysics, 58: 964-977.
Jenner, E., 2002. Azimuthal AVO: Methodology and data examples. The Leading Edge, 21: 782-786.
Liu, E. and Martinez, A., 2012. Seismic fracture characterization : Concepts and practical applications. EAGE, Houten, The Netherlands.
Mahmoudian, F. and Margrave, G.F., 2012. AVAZ inversion for fracture orientation and intensity: a physical modeling study. Extended Abstr., 74th EAGE Conf., Copenhagen.
Martins, J.L., 2006. Elastic impedance in weakly anisotropic media. Geophysics, 71: 2092-2096.
Narr, W., Schechter, W.S. and Thompson, L., 2006. Naturally fractured reservoir characterization: SPE monograph, Richardson, TX, USA.
Pan, X., Zhang, G., Chen, H. and Yin, X., 2017a. McMC-based AVAZ direct inversion for fracture weaknesse. J. Appl. Geophys., 138: 50-61.
Pan, X., Zhang, G., Chen, H. and Yin, X., 2017b. McMC-based nonlinear EIVAZ inversion driven by rock physics. J. Geophys. Engineer., 14: 368-379.
Pšenčík, I. and Gajewski, D., 1998. Polarization, phase velocity and NMO velocity of qP waves in arbitrary weakly anisotropic media. Geophysics, 63: 1754-1766.
Pšenčík, I. and Vavryčuk, V., 1998. Weak contrast PP-wave displacement R/T coefficients in weakly anisotropic elastic media. Pure Appl. Geophys., 151: 699-718.
Pšenčík, I. and Martins, J.L., 2001. Properties of weak contrast PP reflection/ transmission coefficients for weakly anisotropic elastic media. Studia Geophys. Geodaet., 45: 176-199.
Rüger, A., 1997. P-wave reflection coefficients for transversely isotropic models with vertical and horizontal axis of symmetry. Geophysics, 62: 713-722.
Rüger, A., 1998. Variation of P-wave reflectivity with offset and azimuth in anisotropic media. Geophysics, 63: 935-947.
Sacchi, M.D. and Ulrych, T.J., 1995. High-resolution velocity gathers and offset space reconstruction. Geophysics, 60: 1169-1177.
Scales, J.A. and Smith, M.L., 2000. Introductory Geophysical Inverse Theory (draft). Samizdat Press, Golden, CO.
Schoenberg, M., 1980. Elastic wave behavior across linear slip interfaces. J. Acoustical Soc. Am., 68: 1516-1521.
Schoenberg, M., 1983. Reflection of elastic waves from periodically stratified media with interfacial slip. Geophys. Prosp., 31: 265-292.
Schoenberg, M. and Sayers, C.M., 1995. Seismic anisotropy of fractured rock. Geophysics, 60: 204-211.
Shaw, R.K. and Sen, M.K., 2004. Born integral, stationary phase and linearized reflection coefficients in weak anisotropic media. Geophys. J. Internat., 158: 225-238.
Shaw, R.K. and Sen, M.K., 2006. Use of AVOA data to estimate fluid indicator in a vertically fractured medium. Geophysics, 71: C15-C24.
Stolt, R.H. and Weglein, A.B., 1985. Migration and inversion of seismic data. Geophysics, 50: 2458-2472.
Thomsen, L., 1986, Weak elastic anisotropy. Geophysics, 51: 1954-1966.
Thomsen, L., 2002. Understanding seismic anisotropy in exploration and exploitation. SEG 2010 Disting. Instruct. Series, Vol. 5. SEG, Tulsa, OK.
Tsvankin, L., 1996. P-wave signatures and notation for transversely isotropic media: an overview. Geophysics, 61: 467-483.
Tsvankin, L. and Grechka, V., 2011. Seismology of Azimuthally Anisotropic Media and Seismic Fracture Characterization. SEG, Tulsa, OK.

Whitcombe, D.N., 2002. Elastic impedance normalization. Geophysics, 67: 60-62.
Yin, X., Zong, Z. and Wu, G., 2013. Seismic wave scattering inversion for fluid factor of heterogeneous media. Sci. China: Earth Sci., 43: 1934-1942.
Zong, Z., Yin, X. and Wu, G., 2012. AVO inversion and poroelasticity with P- and S-wave moduli. Geophysics, 77: 29-36.
Zong, Z., Yin, X. and Wu, G., 2013. Elastic impedance parameterization and inversion with Young's modulus and Poisson's ratio. Geophysics, 78: N35-42.
Zong, Z., Yin, X., Wu, G. and Wu, Z.P., 2015. Elastic inverse scattering for fluid variation with time-lapse seismic data. Geophysics, 80: WA61-WA67.

APPENDIX A

DERIVATION FOR THE LINEARIZED PP- WAVE REFLECTION COEFFICIENT IN WEAKLY ANISOTROPIC AND HETEROGENEOUS HTI MEDIA

The P-wave polarization and slowness vectors are given by (Shaw and Sen, 2006)

$$\mathrm{t} = \left[\sin\theta\cos\phi, \sin\theta\sin\phi, \cos\theta\right], \tag{A-1}$$

$$\mathrm{t}' = \left[-\sin\theta\cos\phi, -\sin\theta\sin\phi, \cos\theta\right], \tag{A-2}$$

$$\mathrm{p} = 1/\alpha_b\left[\sin\theta\cos\phi, \sin\theta\sin\phi, \cos\theta\right], \tag{A-3}$$

and

$$\mathrm{p}' = 1/\alpha_b\left[-\sin\theta\cos\phi, -\sin\theta\sin\phi, \cos\theta\right]. \tag{A-4}$$

Substituting eqs. (A-1) and (A-2) into eq. (22), then the expression of ξ is given by

$$\xi = \cos^2\theta - \sin^2\theta = \cos 2\theta. \tag{A-5}$$

Thus the expression of η_{mn} can be given by

$$\eta_{11}=\left(\sin^4\theta\cos^4\phi\right)/\alpha_b^2;\qquad \eta_{12}=\left(\sin^4\theta\sin^2\phi\cos^2\phi\right)/\alpha_b^2;$$
$$\eta_{13}=\left(\sin^2\theta\cos^2\theta\cos^2\phi\right)/\alpha_b^2;\qquad \eta_{14}=2\left(\sin^3\theta\cos\theta\sin\phi\cos^2\phi\right)/\alpha_b^2;$$
$$\eta_{15}=2\left(\sin^3\theta\cos\theta\cos^3\right)\phi/\alpha_b^2;\qquad \eta_{16}=2\left(\sin^4\theta\sin\phi\cos^3\phi\right)/\alpha_b^2;$$
$$\eta_{21}=\left(\sin^4\theta\sin^2\phi\cos^2\phi\right)/\alpha_b^2;\qquad \eta_{22}=\left(\sin^4\theta\sin^4\phi\right)/\alpha_b^2;$$
$$\eta_{23}=\left(\sin^2\theta\cos^2\theta\sin^2\phi\right)/\alpha_b^2;\qquad \eta_{24}=2\left(\sin^3\theta\cos\theta\sin^3\phi\right)/\alpha_b^2;$$
$$\eta_{25}=2\left(\sin^3\theta\cos\theta\sin^2\phi\cos\phi\right)/\alpha_b^2;\quad \eta_{26}=2\left(\sin^4\theta\sin^3\phi\cos\phi\right)/\alpha_b^2;$$
$$\eta_{31}=\left(\sin^2\theta\cos^2\theta\cos^2\phi\right)/\alpha_b^2;\qquad \eta_{32}=\left(\sin^2\theta\cos^2\theta\sin^2\phi\right)/\alpha_b^2;$$
$$\eta_{33}=\left(\cos^4\theta\right)/\alpha_b^2;\qquad \eta_{34}=2\left(\sin\theta\cos^3\theta\sin\phi\right)/\alpha_b^2;$$
$$\eta_{35}=2\left(\sin\theta\cos^3\theta\cos\phi\right)/\alpha_b^2;\qquad \eta_{36}=2\left(\sin^2\theta\cos^2\theta\sin\phi\cos\phi\right)/\alpha_b^2;$$
$$\eta_{41}=-2\left(\sin^3\theta\cos\theta\sin\phi\cos^2\phi\right)/\alpha_b^2;\eta_{42}=-2\left(\sin^3\theta\cos\theta\sin^3\phi\right)/\alpha_b^2;\qquad \text{(A-6)}$$
$$\eta_{43}=-2\left(\sin\theta\cos^3\theta\sin\phi\right)/\alpha_b^2;\qquad \eta_{44}=-4\left(\sin^2\theta\cos^2\theta\sin^2\phi\right)/\alpha_b^2;$$
$$\eta_{45}=-4\left(\sin^2\theta\cos^2\theta\sin\phi\cos\phi\right)/\alpha_b^2;\eta_{46}=-4\left(\sin^3\theta\cos\theta\sin^2\phi\cos\phi\right)/\alpha_b^2;$$
$$\eta_{51}=-2\left(\sin^3\theta\cos\theta\cos^3\phi\right)/\alpha_b^2;\qquad \eta_{52}=-2\left(\sin^3\theta\cos\theta\sin^2\phi\cos\phi\right)/\alpha_b^2$$
$$\eta_{53}=-2\left(\sin\theta\cos^3\theta\cos\phi\right)/\alpha_b^2;\qquad \eta_{54}=-4\left(\sin^2\theta\cos^2\theta\sin\phi\cos\phi\right)/\alpha_b^2;$$
$$\eta_{55}=-4\left(\sin^2\theta\cos^2\theta\cos^2\phi\right)/\alpha_b^2;\qquad \eta_{56}=-4\left(\sin^3\theta\cos\theta\sin\phi\cos^2\phi\right)/\alpha_b^2;$$
$$\eta_{61}=2\left(\sin^4\theta\sin\phi\cos^3\phi\right)/\alpha_b^2;\qquad \eta_{62}=2\left(\sin^4\theta\sin^3\phi\cos\phi\right)/\alpha_b^2;$$
$$\eta_{63}=2\left(\sin^2\theta\cos^2\theta\sin\phi\cos\phi\right)/\alpha_b^2;\quad \eta_{64}=4\left(\sin^3\theta\cos\theta\sin^2\phi\cos\phi\right)/\alpha_b^2;$$
$$\eta_{65}=4\left(\sin^3\theta\cos\theta\sin\phi\cos^2\phi\right)/\alpha_b^2;\quad \eta_{66}=4\left(\sin^4\theta\sin^2\phi\cos^2\phi\right)/\alpha_b^2..$$

Substituting eqs. (15), (A-5) and (A-6) into eq. (21) yields

$$
\begin{aligned}
\mathbf{S}(\mathbf{r}_0) &= \Delta\rho\xi + \Delta\boldsymbol{C}\eta_{mn} \\
&= \Delta\rho\cos 2\theta + \frac{\sin^4\theta\cos^4\phi}{\alpha_b^2}\left[\Delta M - \Delta\delta_N M_b\right] \\
&+ \frac{2\sin^4\theta\sin^2\phi\cos^2\phi + 2\sin^2\theta\cos^2\theta\cos^2\phi}{\alpha_b^2}\left[\Delta M - 2\Delta\mu - M_b(1-2g)\Delta\delta_N\right] \\
&+ \frac{\sin^4\theta\sin^4\phi + 2\sin^2\theta\cos^2\theta\sin^2\phi + \cos^4\theta}{\alpha_b^2}\left[\Delta M - M_b(1-2g)^2\Delta\delta_N\right] \\
&- \frac{4\sin^2\theta\cos^2\theta\sin^2\phi}{\alpha_b^2}\Delta\mu - \frac{4\sin^2\theta\cos^2\theta\cos^2\phi}{\alpha_b^2}\left[\Delta\mu - M_b g\Delta\delta_V\right] \\
&+ \frac{4\sin^4\theta\sin^2\phi\cos^2\phi}{\alpha_b^2}\left[\Delta\mu - M_b g\Delta\delta_H\right] + \frac{4\sin^4\theta\sin\phi\cos^3\phi}{\alpha_b^2}\sqrt{g}\Delta\delta_{NH} \\
&+ \frac{4\sin^4\theta\sin^3\phi\cos\phi + 4\sin^2\theta\cos^2\theta\sin\phi\cos\phi}{\alpha_b^2}(1-2g)\sqrt{g}\Delta\delta_{NH} \\
&= \frac{1}{\alpha_b^2}\Delta M - \frac{\sin^2\theta\cos^2\theta}{\alpha_b^2}\Delta\mu + \cos 2\theta\Delta\rho - \frac{M_b}{\alpha_b^2}\left[2g\sin^2\theta\sin^2\phi + 2g\cos^2\theta - 1\right]^2\Delta\delta_N \\
&+ \frac{4M_b g\sin^2\theta\cos^2\phi}{\alpha_b^2}\Delta\delta_V - \frac{4M_b g\sin^4\theta\sin^2\phi\cos^2\phi}{\alpha_b^2}\Delta\delta_H \\
&+ \frac{4M_b\sqrt{g}\sin^2\theta\sin\phi\cos\phi\left[1-2g\left(\sin^2\theta\sin^2\phi + \cos^2\theta\right)\right]}{\alpha_b^2}\Delta\delta_{NH}.
\end{aligned}
\tag{A-7}
$$

Thus the calculation of eq. (20) gives

$$
\begin{aligned}
R_{pp}(\theta,\phi) &= \frac{1}{4M_b\cos^2\theta}\Delta M - \frac{2\sin^2\theta}{M_b}\Delta\mu + \frac{1}{2\rho_b}\left(1 - \frac{1}{2\cos^2\theta}\right)\Delta\rho \\
&- \frac{1}{4\cos^2\theta}\left[2g\sin^2\theta\sin^2\phi + 2g\cos^2\theta - 1\right]^2\Delta\delta_N \\
&+ g\sin^2\theta\cos^2\phi\Delta\delta_V - g\sin^2\theta\tan^2\theta\sin^2\phi\cos^2\phi\Delta\delta_H \\
&+ \sqrt{g}\tan^2\theta\sin\phi\cos\phi\left[1-2g\left(\sin^2\theta\sin^2\phi + \cos^2\theta\right)\right]\Delta\delta_{NH}.
\end{aligned}
\tag{A-8}
$$

In the absence of anisotropy ($\delta_N = \delta_V = \delta_H = \delta_{NH} = 0$), eq. (A-8) reduces to the linearized PP-wave reflection coefficients of an isotropic medium (Zong et al., 2012).

APPENDIX B

ESTIMATION OF FRACTURE SYMMETRY AXIS AZIMUTH BASED ON LSEF METHOD

Rüger (1997, 1998) proposed the linearized PP-wave reflection coefficient for an isotropic half space over an isotropic half space:

$$R_{pp}(\theta,\phi)=\frac{1}{2}\left(\frac{\Delta\rho}{\overline{\rho}}+\frac{\Delta V_p}{\overline{V_p}}\right)+\frac{1}{2}\left\{\frac{\Delta V_p}{\overline{V_p}}-\left(2\frac{\overline{V_s}}{\overline{V_p}}\right)^2\left(\frac{\Delta\rho}{\overline{\rho}}+\frac{2\Delta V_s}{\overline{V_s}}\right)+\left[\Delta\delta^{(V)}+2\left(2\frac{\overline{V_s}}{\overline{V_p}}\right)^2\Delta\gamma\right]\cos^2\phi\right\}\sin^2\theta$$
$$+\frac{1}{2}\left\{\frac{\Delta V_p}{\overline{V_p}}+\Delta\varepsilon^{(V)}\cos^4\phi+\Delta\delta^{(V)}\sin^2\phi\cos^2\phi\right\}\sin^2\theta\tan^2\theta, \qquad \text{(B-1)}$$

The behavior of $R_{pp}(\theta,\phi)$ at small incidence angles is described by the AVO gradient G composed of the azimuthally invariant part G_{iso} and the anisotropic contribution G_{ani} multiplied with the squared cosine of the azimuthal angle ϕ with the symmetry axis. If the symmetry-axis orientation is unknown, ϕ should be formally expressed by the difference between the azimuthal direction ϕ_{obs} of observed azimuth and the direction of the symmetry-axis plane ϕ_{sym}. Thus for the case of small angles of incidence, the linearized PP-wave reflection coefficient in terms of AVO intercept P and gradient G can be written as

$$R_{pp}(\theta,\phi_{obs})=P+G(\phi_{obs}-\phi_{sym})\sin^2\theta, \qquad \text{(B-2)}$$

where $G(\phi_{obs}-\phi_{sym})=G_{iso}+G_{ani}\cos^2(\phi_{obs}-\phi_{sym})$ represents the AVO gradient measured at azimuth ϕ_{obs}. Thus the azimuthal gradient can be then expressed as

$$G(\phi_{obs}-\phi_{sym})=A_G+B_G\cos\left(2(\phi_{obs}-\phi_{sym})\right), \qquad \text{(B-3)}$$

where $A_G=G_{iso}\sin^2\theta+G_{ani}\sin^2\theta/2$ and $B_G=G_{ani}\sin^2\theta/2$. In a weakly anisotropic medium, the azimuthal gradient varies with the cosine function when the angle of incidence is fixed. The cosine curve is approximated as an ellipse in a polar coordinate, in which A_G+B_G and A_G-B_G represent the semi-major axis and the semi-minor axis, respectively.

Based on the LSEF method, the fracture intensity and orientation in reservoirs can be estimated using the azimuthal gradients, in which the ellipticity indicates the anisotropic intensity or the fracture density, and the semi-axis of ellipse indicate the fracture orientation. However, this introduces a 90 degree ambiguity into the estimate of the fracture symmetry axis azimuth, and the incorporation of the a priori knowledge about the fracture orientation may effectively eliminate the ambiguity.

APPENDIX C

PARAMETERIZATION FOR THE FRACTURE WEAKNESS REFLECTIVITY

Assuming $R_{\delta_N^r} = R_{\delta_N}$, i.e., $\frac{1}{2}\left(\frac{\Delta\delta_N^r}{\delta_{N0}^r}\right) = \frac{1}{2}\Delta\delta_N$, then it gives

$$d\delta_N = d\left(\frac{\delta_N^r}{\delta_{N0}^r}\right), \tag{C-1}$$

where the subscript 0 represents the average quantities, and $\Delta\delta_N^r = \delta_{N2}^r - \delta_{N1}^r$ indicates the changes of the parameter δ_N^r across the interface. Taking the integral on eq. (C-1), the calculation of eq. (C-1) then yields

$$\int d\delta_N \cdot \delta_{N0}^r = \int d\delta_N^r. \tag{C-2}$$

The evaluation of eq. (C-2) then yields

$$\delta_N^r = \delta_{N0}^r \cdot \delta_N + C, \tag{C-3}$$

where C is a constant. δ_N^r indicates the first-order expression of δ_N, and it can be written as

$$\delta_N^r = m \cdot \delta_N + n, \tag{C-4}$$

where m and n are two unknown quantities. Substituting eq. (C-3) into eq.(C-4), the two unknown quantities can be written as

$$n = m\left(1-\delta_{N0}\right) = C, \tag{C-5a}$$

and

$$m = \frac{C}{1-\delta_{N0}}. \tag{C-5b}$$

Substituting eq. (C-5) into eq. (C-4) yields

$$\delta_N^r = \frac{C}{1-\delta_{N0}}\left(\delta_N + 1 - \delta_{N0}\right). \tag{C-6}$$

For simplicity, C can be valued to unit, eq. (C-6) then gives

$$\delta_N^r = \frac{1}{1-\delta_{N0}}\left(\delta_N + 1 - \delta_{N0}\right). \tag{C-7}$$

Similarly, assuming that $R_{\delta_T^r} = R_{\delta_T}$ and similar expression of the anisotropic parameters can be also obtained written as

$$\delta_T^r = \frac{1}{1-\delta_{T0}}\left(\delta_T + 1 - \delta_{T0}\right). \tag{C-8}$$